Activation of Methane and Carbon Dioxide Mediated by Transition-Metal Doped Magnesium Oxide Clusters [MMgO]+/0/− (M=Sc–Zn)

ARTICLE *in* CHEMISTRY - A EUROPEAN JOURNAL · APRIL 2015

Impact Factor: 5.73 · DOI: 10.1002/chem.201500715 · Source: PubMed

4 AUTHORS, INCLUDING:

Patricio Gonzalez-Navarrete
Technische Universität Berlin
20 PUBLICATIONS **181** CITATIONS
SEE PROFILE

Maria Schlangen
Technische Universität Berlin
97 PUBLICATIONS **1,332** CITATIONS
SEE PROFILE

ChemPubSoc Europe

DOI: 10.1002/chem.201500715

CHEMISTRY
A European Journal
Full Paper

Density Functional Calculations

Activation of Methane and Carbon Dioxide Mediated by Transition-Metal Doped Magnesium Oxide Clusters $[MMgO]^{+/0/-}$ (M = Sc–Zn)

Jilai Li,[a, b] Patricio González-Navarrete,[a] Maria Schlangen,[a] and Helmut Schwarz*[a]

The reaction enthalpies for the activation of CH_4 and CO_2 mediated by heteronuclear magnesium oxide clusters $[MMgO]^{+/0/-}$ (M = Sc–Zn) in different charge states have been systematically evaluated by means of density functional theory (DFT). Thermodynamic trends have been elucidated. Regarding the activation of methane, those mixed cluster oxides that contain a late 3d transition metal are in general more promising; in contrast, clusters doped with an early 3d transition metal are predicted to be more suitable for CO_2 activation. The effects of the charge of the cluster and the oxidation states of the metals M towards both the activation of CH_4 and of CO_2 have also been addressed. Promising reagents, such as $[MMgO_2]^+$ (M = Cu, Zn) for methane activation, are recommended based on a systematic and comprehensive analysis of thermodynamic and kinetic properties. Finally, based on the evaluation of the individual reactions, the task of identifying "simple" reagents with a single reactive site that could mediate efficiently the industrially important coupling of CH_4 and CO_2 to CH_2CO seems extremely challenging.

1. Introduction

Carbon dioxide reforming of methane (CRM), that is, the generation of "syngas" from CO_2 and CH_4, first proposed by Fischer and Tropsch in 1928,[1] is still quite attractive as it represents an interesting route to utilize two cheap and abundantly available C1 sources to generate higher value products.[2] However, CRM reactions and related processes are highly endothermic. For example, the direct coupling of methane and CO_2, giving rise to acetic acid ($CH_4 + CO_2 \rightarrow CH_3COOH$), is endothermic with $\Delta_r H$ (298 K) = 36.5 kJ mol^{-1},[3] making this process thermochemically unfavorable. As a result, no procedure currently exists to bring about this seemingly simple process in an environmentally benign and economically feasible manner. In addition, concepts to help in the rational design of catalysts for CRM are by and large missing.[2b,4]

Magnesium oxide has proved as a highly promising material because it exhibits decent to good reactivity for quite a few industrially important reactions, as for example the reduction of CO_2,[5] oxidative coupling of methane (OCM),[6] and CRM.[6c,7] Interestingly, the reactivity of various magnesium oxides has been found to increase upon doping by metals, as demonstrated, for example, for OCM over Li-doped magnesium oxides,[8] in which the lithium element plays a pivotal role by changing the properties of the catalyst.[8b] However, metal-doped magnesium oxides are catalytically unstable and easily deactivated because of the poor sintering resistance and serious problems of coking. Even though extensive studies have been carried out, the true nature of the active sites as well as the actual reaction mechanisms of such doped magnesium oxide catalysts are still unknown, and controversial interpretations do exist.[9] Therefore, a better understanding of the questions related to the fundamental aspects underlying the activation and coupling of methane and carbon dioxide at a molecular level is highly indicated.

Motivated by these issues, we decided to systematically investigate by computational means the reactivity of 3*d* transition-metal doped magnesium oxide clusters in their positive, neutral, and negative charge states $[M_xMg_yO_z]^{+/0/-}$ (M = Sc–Zn; $x = y = z = 1$) towards CH_4 and CO_2 as a first step to eventually addressing features relevant for the coupling of these two C1 units. The effects of the 3d transition metals, as well as the role of the charges of the clusters, were elucidated for reactions (1)–(11) (See Scheme 1). By state-of-the-art theoretical methods, in a screening procedure, we aimed to identify the thermodynamically most promising candidates of the cluster oxides.[10]

$$[MMgO]^{+/0/-} + CH_4 \rightarrow [MMgOH]^{+/0/-} + CH_3^{\cdot} \quad (1)$$

$$[MMgO]^{+/0/-} + CH_4 \rightarrow [MMg]^{+/0/-} + CH_3OH \quad (2)$$

$$[MMgO]^{+/0/-} + CH_4 \rightarrow [MMgCH_2]^{+/0/-} + H_2O \quad (3)$$

$$[MMgO]^{+/0/-} + CH_4 \rightarrow [MMgCH_2O]^{+/0/-} + H_2 \quad (4)$$

$$[MMg]^{+/0/-} + CH_4 \rightarrow [MMgCH_2]^{+/0/-} + H_2 \quad (5)$$

[a] Dr. J. Li, Dr. P. González-Navarrete, Dr. M. Schlangen, Prof. Dr. H. Schwarz
Institut für Chemie, Technische Universität Berlin
Straße des 17. Juni 135, 10623 Berlin (Germany)
E-mail: Helmut.Schwarz@tu-berlin.de

[b] Dr. J. Li
Institute of Theoretical Chemistry, Jilin University
Changchun 130023 (P. R. China)

Supporting information for this article is available on the WWW under http://dx.doi.org/10.1002/chem.201500715.

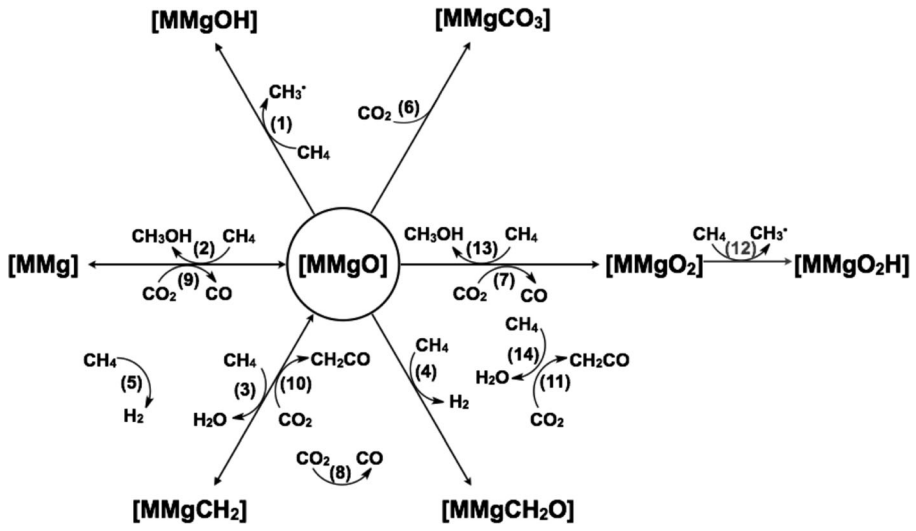

Scheme 1. The network for the activation and coupling of CO_2 and CH_4 mediated by $[M_xMg_yO_2]^{+/0/-}$.

$$[MMgO]^{+/0/-} + CO_2 \rightarrow [MMgCO_3]^{+/0/-} \quad (6)$$

$$[MMgO]^{+/0/-} + CO_2 \rightarrow [MMgO_2]^{+/0/-} + CO \quad (7)$$

$$[MMgCH_2]^{+/0/-} + CO_2 \rightarrow [MMgCH_2O]^{+/0/-} + CO \quad (8)$$

$$[MMg]^{+/0/-} + CO_2 \rightarrow [MMgO]^{+/0/-} + CO \quad (9)$$

$$[MMgCH_2]^{+/0/-} + CO_2 \rightarrow [MMgO]^{+/0/-} + CH_2CO \quad (10)$$

$$[MMgCH_2O]^{+/0/-} + CO_2 \rightarrow [MMgO_2]^{+/0/-} + CH_2CO \quad (11)$$

In addition to the study of reactions (1)–(11), we also considered three processes [reactions (12)–(14)] in which higher oxidized species $[MMgO_2]$ are involved in hydrogen atom transfer (HAT), oxygen atom transfer (OAT), and in the generation of metal–carbene oxides. We will comprehensively present the derived trends of reaction enthalpies and structural data. The results show how the nature of the 3d transition metals, the charge, and the oxidation states affect the reactivities of doped metal-oxide cluster catalysts.

$$[MMgO_2]^{+/0/-} + CH_4 \rightarrow [MMgO_2H]^{+/0/-} + CH_3^{\cdot} \quad (12)$$

$$[MMgO_2]^{+/0/-} + CH_4 \rightarrow [MMgO]^{+/0/-} + CH_3OH \quad (13)$$

$$[MMgO_2]^{+/0/-} + CH_4 \rightarrow [MMgCH_2O]^{+/0/-} + H_2O \quad (14)$$

2. Results

2.1 Geometries

The lowest-energy geometries obtained at the DFT-B3LYP/Q level of theory for all of the educts and product ions involved in reactions (1)–(14) (except $[MMg]^{+/0/-}$) are shown in Figure 1 and given in Table S1 in the Supporting Information; the spin multiplicities for each structure are given in Table S2 in the Supporting Information.

For all heteronuclear MMgO monoxides, as well as for the Mg_2O species, the calculations converged to μ bridging oxides, $[Mg(\mu\text{-}O)M]^{+/0/-}$, in a linear (**1.1**) and/or a bent (**1.2**) fashion (Figure 1 and Table S1). For most of the cations and anions, the structures are linear, except for cationic $[CoMgO]^+$ and $[NiMgO]^+$, and anionic $[NiMgO]^-$ oxides. In contrast, the neutral cluster oxides have been predicted to possess a bent configuration in most cases, except for $[Mg_2O]^0$, $[CrMgO]^0$, and $[MnMgO]^0$ (Table S1).

Regarding the higher oxidized cluster, all $[MMgO_2]$ species prefer a $[M(\mu\text{-}O)_2Mg]^{+/0/-}$ structure (**4.1**) with only two exceptions, $[VMgO_2]^-$ and $[CrMgO_2]^-$; these dioxides possess a zigzag structure $[MMg(\mu\text{-}O)O]^{+/0/-}$ with a terminal oxygen atom bound to the transition metal (**4.2**; Figure 1).

We also considered several structures for the products [MMgOH] (**2.1**, **2.2**, **2.3**, and **2.4**), $[MMgO_2H]$ (**5.1**, **5.2**, **5.3** and **5.4**), $[MMgCH_2]$ (**3.1**), $[MMgCH_2O]$ (**6.1**, **6.2**, and **6.3**), and $[MMgCO_3]$ (**7.1** to **7.7**; Figure 1). Detailed structural and energetic descriptions are given in the Supporting Information.

2.2 Thermodynamic and periodic trends

As shown in Scheme 1 for the reaction using [MMgO] as the starting reagent, 14 reactions have been considered in this study; they can be classified ito two categories: i) Activation of CH_4 or CO_2, and ii) coupling of the two molecules to produce the acetic acid equivalent CH_2CO. The reaction enthalpies of processes (1)–(14) are given in Table 1 and plotted in Figures 2 and 3, respectively.

2.2.1 Reactions with CH_4

Four possibilities were considered regarding the activation of CH_4 (Scheme 1): i) HAT to the oxides giving rise to a methyl radical [$CH_3^{\cdot}$; reactions (1) and (12)]; ii) OAT from the oxides to methane, resulting in the generation of methanol [reactions (2) and (13)]; iii) twofold C–H bond activation accompanied with the formation of a carbene complex and of water [reactions (3) and (14)]; and iv) dehydrogenation of CH_4 [reactions (4) and (5)].

As shown in Figure 2, the following trends were found:

i) The enthalpies ($\Delta_r H$) for reactions (1)–(3) and (12)–(14) (Figure 2a–f) decrease by and large in changing the dopant metal M from left to right across the periodic table. Considering the same charge state, for those [MMgO] and

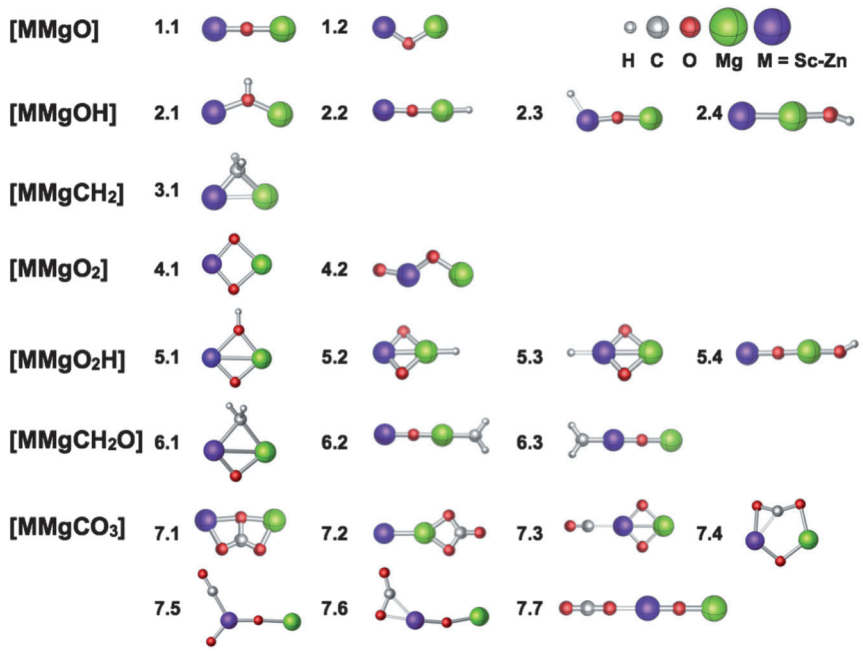

Figure 1. Lowest-energy structures of [MMgO], [MMgOH], [$MMgCH_2$], [$MMgO_2$], [$MMgO_2H$], [$MMgCH_2O$], and [$MMgCO_3$] as obtained at the B3LYP/Q level of theory; M = Sc–Zn (see the Supporting Information, Tables S1 and S2 for details).

[$MMgO_2$] cluster oxides containing early 3d transition metals the reaction endothermicities are predicted to be much higher than those containing late 3d transition metals. Furthermore, the endothermicities of the reactions are generally smaller for the cationic species than those for their anionic counterparts. However, this does not hold true for reaction (1) or reaction (12) when the clusters contain early 3d transition metals; both processes correspond to HAT.

ii) The effects of the charges of the systems do not entail significant changes in the reaction enthalpies for the systems that contain early to middle 3d transition metals; however, for heteronuclear cluster oxides containing late 3d transition metals, charge effects are more pronounced.

iii) The enthalpies of the reaction of the cluster dioxides $[MMgO_2]^{+/0/-}$ with methane are remarkably lower than those calculated for the mono-oxides $[MMgO]^{+/0/-}$; this indicates that higher oxidized metal-oxides may be more suitable in these reactions. In particular, for the HAT and OAT processes [reactions (12) and (13)] the reaction enthalpies are even exothermic for some cluster oxides when doped with late 3d transition metals.

iv) For the processes involving the release of H_2 [reactions (4) and (5)], an opposite trend has been found regarding the role of the doping metal M, that is, the reaction enthalpies increase from left to right across the periodic table. Furthermore, anionic oxides containing early 3d transition metals might be more promising candidates to mediate these conversions. In particular, dehydrogenation according to $[MMg]^{+/0/-} + CH_4 \rightarrow [MMgCH_2]^{+/0/-} + H_2$ [reaction (5)] is exothermic for the $[ScMg]^-/CH_4$ couple.

v) Dehydrogenation of methane accompanied with the formation of water [reactions (3) and (14)] is more endothermic than the release of hydrogen [reactions (4) and (5)]. This holds true in particular for those heteronuclear cluster oxides containing early 3d transition metals reflecting their high oxygen-atom affinity (OAA).

2.2.2 Reactions with CO_2

For the reactions with CO_2, as depicted in Scheme 1, three types of processes have been considered: i) Adsorption of CO_2 [reaction (6)]; ii) OAT from CO_2 associated with the elimination of CO [reactions (7)–(9)]; and iii) generation of CH_2CO [reactions (10) and (11)]. The data represented in Figure 3 reveal how these processes are affected by the nature of the doping metal and the charge states of the heteronuclear cluster oxides.

As shown in Figure 3, some general trends can be noted:

The chemi- or physisorption of CO_2 to the cluster [reaction (6)], in which different isomers of $[MMgCO_3]^{+/0/-}$ are generated (see below), is exothermic for all charged and neutral $[MMgO]^{+/0/-}$ oxides. Furthermore, CO_2 adsorption to anionic oxides containing a late 3d transition metal have been calculated to be much more exothermic than those of their cationic and neutral analogues. This observation is in good agreement with the general trend noted earlier for CO_2 activation, whereby anionic systems exhibit higher reactivities toward CO_2 capture.[11] In contrast, the cationic and neutral species display similar exothermicities; however, some exceptions are noted for M = Sc, Ti, and Mn.

Reactions (7)–(11) become less exothermic when the metal M changes from left to the right across the periodic table; clearly, $[MMgO]^{+/0/-}$ oxides containing late 3d transition metals are less favorable for the reduction of CO_2. This trend agrees well with the available experimental data for OAT from CO_2 to $[M]^-$ and $[MO]^-$, respectively (see the Supporting Information, Figure S1).[3]

For processes (7)–(11), anionic candidates give rise to more exothermic reactions as computed for their cationic counterparts; this is particularly striking for the reduction of CO_2 by $[MMg]^-$ [reaction (9)].

Table 1. Reaction enthalpies (kJ mol^{-1}) for reactions (1)–(14).

Reaction	Charge state	M =	Mg	Sc	Ti	V	Cr	Mn	Fe	Co	Ni	Cu	Zn
	+		130	165	170	172	113	169	156	97	79	69	66
(1)	0		137	158	161	153	142	132	134	97	54	19	95
	−		147	178	157	133	166	138	134	120	126	95	120
	+		165	386	364	252	131	263	185	78	50	25	53
(2)	0		157	421	353	278	246	267	212	146	113	81	39
	−		284	533	415	328	320	397	263	267	232	102	207
	+		214	312	293	270	177	219	192	119	100	83	130
(3)	0		254	345	334	266	226	227	205	175	160	133	182
	−		269	368	354	289	257	270	241	190	158	157	219
	+		214	55	77	96	134	156	154	156	148	205	155
(4)	0		149	87	85	71	155	113	111	123	124	157	114
	−		173	121	96	81	113	121	115	108	120	141	160
	+		162	39	42	131	159	69	119	154	163	170	190
(5)	0		209	36	94	100	92	72	105	142	160	165	255
	−		98	−53	51	74	50	−14	91	36	38	167	125
	+		−115	−218	−114	−96	−106	−68	−78	−113	−142	−141	−96
(6)	0		−144	−123	−188	−117	−94	−115	−84	−97	−136	−117	−103
	−		−151	−185	−172	−204	−114	−116	−108	−194	−236	−269	−161
	+		151	−138	−116	−51	9	71	95	97	171	264	220
(7)	0		62	−129	−150	−106	9	44	34	46	66	142	118
	−		68	−108	−129	−109	−32	38	22	13	35	124	126
	+		62	−193	−153	−111	20	−1	26	100	111	186	88
(8)	0		−41	−195	−186	−131	−8	−51	−31	11	26	87	−5
	−		−32	−183	−195	−145	−81	−86	−63	−20	25	48	4
	+		11	−210	−188	−76	45	−87	−10	98	126	151	123
(9)	0		18	−245	−178	−102	−70	−91	−36	30	63	95	136
	−		−108	−357	−239	−152	−144	−221	−87	−91	−57	73	−31
	+		−36	−133	−115	−92	1	−41	−14	59	78	96	48
(10)	0		−76	−166	−156	−87	−48	−48	−26	3	18	45	−3
	−		−91	−189	−175	−111	−79	−92	−63	−12	20	22	−41
	+		53	−78	−77	−32	−10	31	56	55	138	173	180
(11)	0		28	−101	−120	−61	−31	47	38	39	57	100	119
	−		10	−114	−109	−75	−30	32	21	20	30	98	81
	+		−37	198	220	147	80	68	37	11	−42	−47	−43
(12)	0		89	135	131	139	135	107	122	129	116	−36	−18
	−		102	116	118	131	126	124	125	124	125	83	−11
	+		25	313	292	227	167	105	81	79	5	−88	−44
(13)	0		114	305	326	281	167	132	142	130	110	34	58
	−		108	284	305	285	208	138	154	163	141	52	50
	+		126	256	256	210	188	148	122	123	41	5	−2
(14)	0		151	279	298	240	209	132	140	140	121	79	59
	−		169	292	288	253	208	146	157	158	148	80	97

3. Discussion

3.1 Geometries

The structural deviations observed for the three charge states of $[MMgO]^{+/0/-}$, that is, bent or linear structures, can be interpreted in terms of an electronic structure analysis. As a representative example, the frontier orbitals of the $[ScMgO]^{+/0/-}$ oxides are given in Figure 4. As depicted in Figure 4, the three doubly occupied oxygen *p* orbitals possess similar shapes for all three charge states of the cluster oxides. The same holds true for the d_{z^2} and s orbitals of Sc and Mg, respectively, in the case of the cationic and anionic species in which these orbitals are singly occupied in the former and doubly occupied in the latter (Figure 4). However, upon addition of one electron to

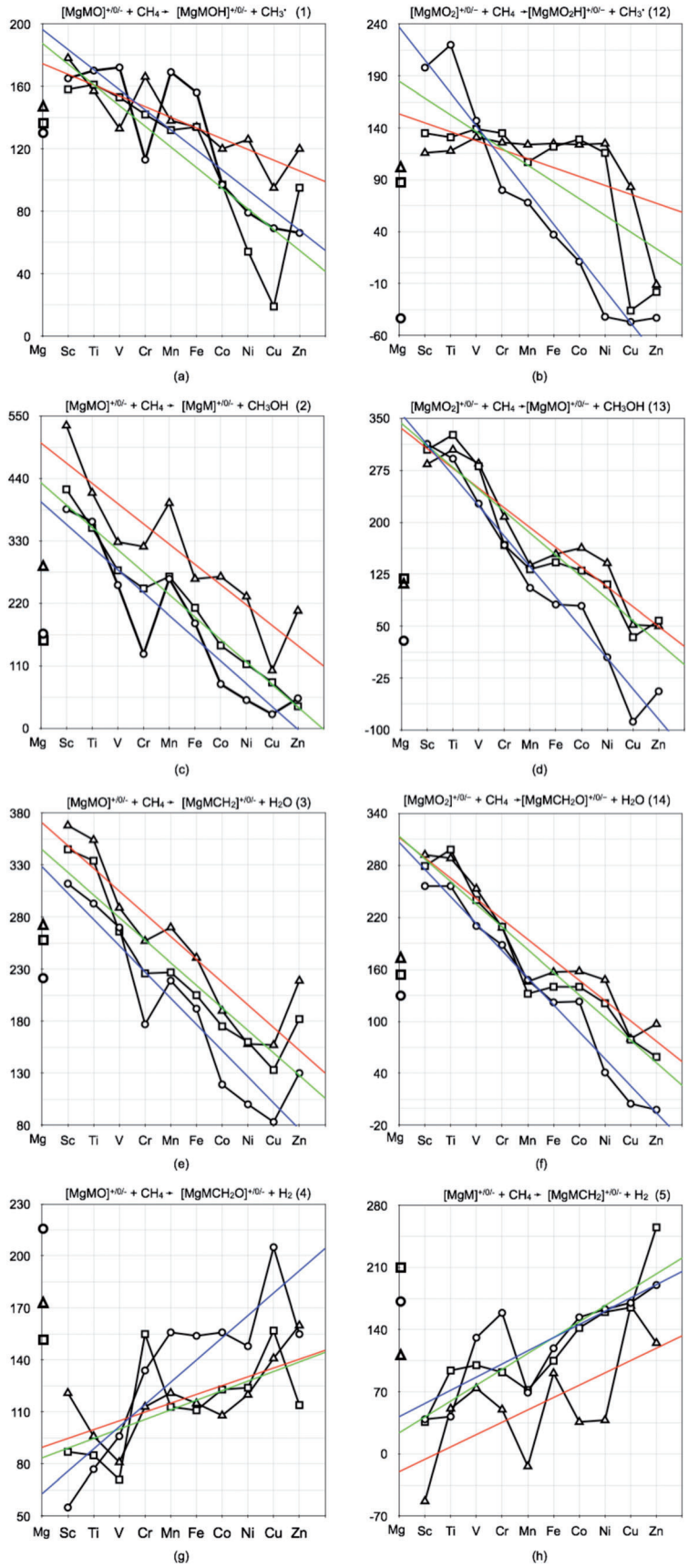

the singly occupied d_{z^2} orbital of the cationic species, the d_{z^2} orbital together with the s orbital of Mg form two hybrid orbitals with 94% overlap, occupied by two antiferromagnetically coupled electrons; notably, all bent neutral [MMgO] species possess this pair of hybrid orbitals. Thus, the structural changes upon addition/removal of an electron to/from the neutral clusters mostly affect the covalent d–s interactions between M and Mg.

3.2 Reactions with methane

Spin density at the abstracting main-group atom, for example a terminal oxygen atom in gaseous oxo-clusters, plays a crucial role in HAT processes,[4a,10,12] including oxides containing first-row transition metals.[12a–c,e,f,i–k,12] As indicated by quantum chemical calculations, all oxide species which are capable of HAT from methane possess a high spin density at a terminal oxygen atom to which the hydrogen atom is transferred. In contrast, spin density at a metal atom has been found irrelevant for HAT.[13] Based on this, we looked into the relationship between the HAT reactivity and the spin density distributions in the precursors $[MMgO]^{+/0/-}$ and $[MMgO_2]^{+/0/-}$. As shown in Table 2, the largest spin densities are located at the transition metals or the Mg atom in most of the species analyzed, whereas the spin densities on the oxygen atom(s) have been found to be considerably smaller. Furthermore, none of the doped magnesium oxide clusters possess a terminal oxygen atom at which a high spin density is located. In line with the asserted correlation between an oxygen-centered radical and HAT reactivity, the transfer of a hydrogen atom to the cluster oxides is endothermic for all monoxide clusters and for almost all dioxide clusters investigated in this study (see Figure 2a,b and Table 1); the cationic dioxides $[NiMgO_2]^+$, $[CuMgO_2]^+$, and $[ZnMgO_2]^+$, as well as neutral $[CuMgO_2]$ and $[ZnMgO_2]$ and anionic $[ZnMgO_2]^-$, constitute the only exceptions, in which the spin density is mainly localized on the oxygen atom.

Nevertheless, the oxygen atoms of cationic $[MMgO]^+$ and $[MMgO_2]^+$ are more favorable sites for HAT, except in $[ScMgO]^+$, $[TiMgO]^+$, $[VMgO]^+$, and $[ZnMgO]^+$; HAT gives rise to $[M(\mu\text{-OH})Mg]^+$ (**2.1**) and $[M(\mu\text{-O})(\mu\text{-OH})Mg]^+$ (**5.1**). Furthermore, regarding the neutral and anionic clusters, the Mg atoms are the

Figure 2. Reaction enthalpies for the reactions involving CH_4: a) Reaction (1); b) reaction (12); c) reaction (2); d) reaction (13); e) reaction (3); f) reaction (14); g) reaction (4); h) reaction (5), as obtained at DFT-B3LYP/Q level of theory. Cations: ○; neutral species: □; anions: △. General trends of the reactions are shown in blue, green, and red straight lines, respectively. Enthalpies are corrected for ZPVE contributions and given in kJ mol^{-1}.

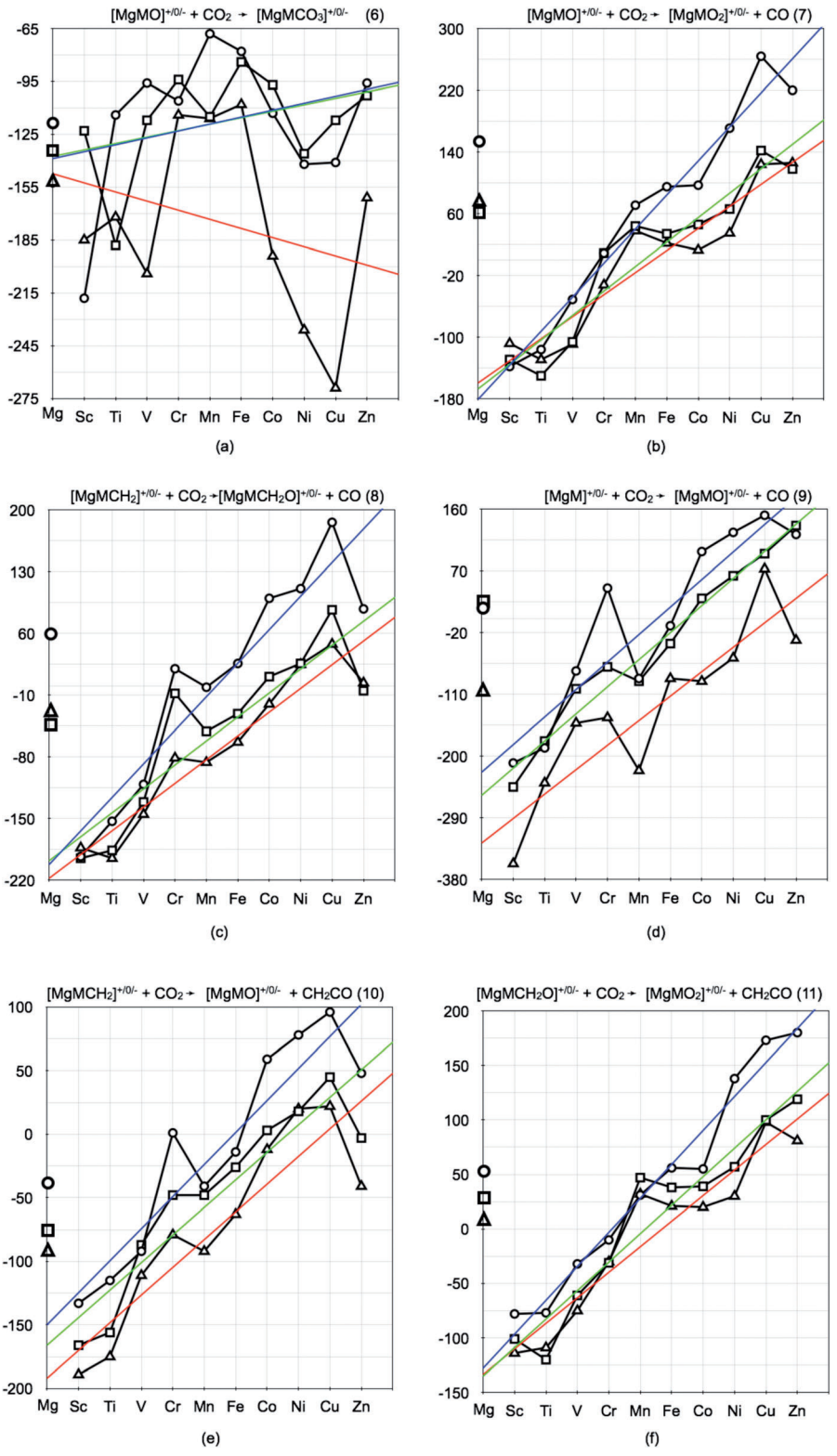

Figure 3. Reaction enthalpies for the reactions with CO_2: a) Reaction (6); b) reaction (7); c) reaction (8); d) reaction (9); e) reaction (10); f) reaction (11), as obtained at DFT-B3LYP/Q level of theory. Cations: ○; neutral species: □; anions: △. To aid the eye, trends of the reactions are shown in blue, green, and red straight lines. Enthalpies are corrected for ZPVE contributions and given in kJ mol^{-1}.

thermochemically preferred sites to abstract a hydrogen atom, giving rise to species having a Mg–H bond in $[M(\mu\text{-}O)MgH]^{0/-}$ (**2.2**) and $[M(\mu\text{-}O)_2MgH]^{0/-}$ (**5.2**).

Local charge is an additional factor that can dramatically influence C–H bond activation.[12p] Previous studies have suggested that a large positive local charge around the hydrogen abstracting center generally enables higher HAT reactivity.[12p,14] However, no correlation could be established between atomic charge values and the hydrogen abstracting atoms (Table 3), indicating that other factors such as, for example, electronic properties affect the HAT process.

3.3 Reactions with CO_2

The general picture for the activation of CO_2 shows that the presence of a negative charge may play an important role in promoting the carboxylation.[11,15] To reveal the nature of the CO_2 activation step, we examined the relationship between the local charge distribution of the [MMgO] cluster oxides (Table 3) with the most stable structures of the $[MMgCO_3]^{0/+/-}$ isomers generated according to reaction (6); this process is exothermic for all three charge states.

Regarding the anionic species $[MMgO]^-$, for those oxide clusters that possess a highly negative charge on the oxygen atom (from −1.56 to −2.07 for M = Mg, Cr, Mn, Co, Ni, Cu, Zn), the most stable structure of the $[MMgCO_3]^-$ isomers corresponds to a carbonate structure (**7.1** or **7.2**), whereas those with a less negative charge on the oxygen atom (from 1.32 to 1.50 for M = Sc, Ti, V, Fe) prefer alternative structures (e.g., **7.3**, **7.5**, and **7.6**). With respect to the cationic and anionic $[MMgCO_3]^{0/+}$ isomers, the carbonate structure **7.1** corresponds likewise to the most stable isomer with M = Mg, Cr, Mn, Co, Ni, Cu, or Zn (with only $[MnMgO]^+$ as an exception), whereas for the cluster

Table 2. The spin densities (in e bohr^{-3}) of $[MMgO]^{+/0/<M->}$ and $[MMgO_2]^{+/0/<M->}$ as derived from a QTAIM analysis.

Charge State	Atom	M=	Mg	Sc	Ti	V	Cr	Mn	Fe	Co	Ni	Cu	Zn
						MMgO							
	O		0.10	0.11	0.07	−0.17	0.18	0.27	0.34	0.14	0.21	0.00	0.20
+	Mg		0.45	0.93	0.90	0.93	0.54	0.65	0.70	−0.49	−0.34	0.00	0.29
	M		0.45	0.95	2.03	3.24	4.28	5.09	3.96	2.36	1.13	0.00	0.51
	O		0.11	0.08	−0.04	−0.22	0.09	0.25	0.26	0.22	0.27	0.04	0.26
0	Mg		0.95	0.61	0.54	−0.34	0.95	0.95	0.74	0.76	0.75	0.94	0.95
	M		0.95	0.31	1.50	3.56	4.96	5.80	3.00	2.03	0.98	0.01	0.79
	O		0.00	0.00	−0.03	−0.03	0.01	0.15	0.13	0.29	0.07	0.00	0.00
−	Mg		0.50	0.00	−0.01	−0.01	0.01	−0.38	−0.31	−0.45	0.34	0.00	0.56
	M		0.50	0.00	1.04	2.04	4.98	4.23	3.18	2.16	0.58	0.00	0.44
						$MMgO_2$							
	O1		0.50	0.00	−0.02	0.01	0.02	0.12	0.06	0.05	0.73	0.70	0.50
	O2		0.50	0.00	−0.02	0.01	0.02	0.12	0.06	0.05	0.73	0.97	0.50
+	Mg		0.00	0.00	0.06	0.01	−0.05	−0.06	0.03	−0.01	−0.01	−0.09	0.00
	M		0.00	0.00	0.97	1.96	3.01	3.82	2.85	1.90	1.56	0.41	0.01
	O1		0.00	0.07	0.03	0.03	−0.06	0.12	0.35	0.38	0.30	0.34	0.00
	O2		0.00	0.07	0.03	0.03	−0.06	0.12	0.35	0.38	0.30	0.34	0.00
0	Mg		0.00	0.71	0.85	0.84	0.13	−0.03	−0.10	−0.13	−0.04	−0.01	0.00
	M		0.00	0.14	1.09	2.11	3.98	4.80	3.40	2.36	1.44	0.34	0.00
	O1		0.09	0.07	−0.03	−0.09	0.00	0.14	0.31	0.23	0.35	0.39	0.20
	O2		0.09	0.01	−0.03	0.03	−0.08	0.14	0.31	0.23	0.35	0.39	0.20
−	Mg		0.41	0.90	0.89	−0.23	0.01	0.84	0.81	−0.83	0.88	0.86	0.46
	M		0.41	1.02	0.18	2.29	3.07	4.88	3.57	2.37	1.42	0.35	0.13

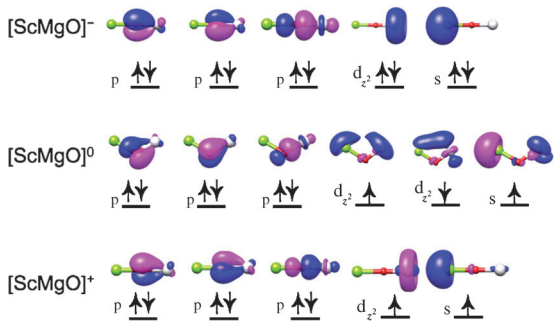

Figure 4. Schematic frontier orbital diagrams of $[ScMgO]^{+/0/-}$.

oxides with M = Sc, Ti, V, or Fe, the structures **7.3**, **7.4**, **7.6** and **7.7** are preferred. However, the local charge distribution of the cationic and neutral cluster oxides $[MMgO]^{0/+}$ are not correlated with these observations. Moreover, we could not identify other common properties like, for example, the formal oxidation state of the 3d transition metal as a determining factor in forming the most stable $[MMgCO_3]^{0/+/-}$ isomer. Thus, it is not possible to assign a single factor as the cause for a particular isomer preference.

3.4 On the coupling of CH_4 and CO_2

Among the reactions (1)–(14) shown in Scheme 1, three catalytic cycles can be envisioned: i) [MMgO]→[MMg]→

Table 3. The QTAIM atomic charges of $[MMgO]^{+/0/<M->}$.

Charge State	Atom	M=	Mg	Sc	Ti	V	Cr	Mn	Fe	Co	Ni	Cu	Zn
	O		−1.97	−1.76	−1.26	−1.44	−1.84	−1.87	−1.30	−1.80	−1.27	−1.65	−1.78
+	Mg		1.49	1.03	0.97	1.03	1.41	1.30	1.16	1.45	1.42	1.74	1.65
	M		1.49	1.74	1.28	1.41	1.43	1.57	1.14	1.34	0.85	0.92	1.13
	O		−1.97	−1.74	−1.34	−1.52	−1.73	−1.88	−1.44	−1.32	−1.26	−1.59	−1.75
0	Mg		0.99	0.69	0.63	0.75	0.99	0.99	0.81	0.86	0.86	0.99	0.99
	M		0.99	1.05	0.72	0.77	0.74	0.89	0.63	0.46	0.40	0.60	0.76
	O		−2.07	−1.48	−1.32	−1.50	−1.75	−1.94	−1.43	−1.75	−1.56	−1.98	−2.01
−	Mg		0.53	0.08	0.02	0.07	0.08	0.42	0.27	0.48	0.39	0.44	0.59
	M		0.53	0.40	0.30	0.43	0.67	0.52	0.15	0.26	0.17	0.54	0.42

$[MMgCH_2]\rightarrow[MMgO]$ [reactions (2), (5),and (10)], ii) $[MMgO_2]\rightarrow[MMgO]\rightarrow[MMgCH_2O]\rightarrow[MMgO_2]$ [reactions (13), (4), and (11)], and iii) $[MMgO]\rightarrow[MMg]\rightarrow[MMgCH_2]\rightarrow[MMgCH_2O]\rightarrow[MMgO_2]\rightarrow[MMgO]$ [reactions (2), (5), (8), (11), and (13)]. In these cycles, both CH_4 and CO_2 are consumed, giving rise to H_2, CH_2CO, CO and CH_3OH. The net process of the two former cycles corresponds to $2\,CH_4+CO_2\rightarrow H_2+CH_2CO+CH_3OH$, which, with a reaction enthalpy of 291 kJ mol^{-1}, is too endothermic to have any practical relevance. This also holds true for the third cycle, with the net process $3\,CH_4+2\,CO_2\rightarrow H_2+CH_2CO+2CH_3OH+CO$; this has an even greater overall reaction enthalpy of 467 kJ mol^{-1}. On considering that the reaction $CH_4+CO_2+XO\rightarrow CH_2O+H_2O+CO+X$ is exothermic (-81.9 kJ mol^{-1}) when using N_2O ($X=N_2$) for the regeneration of the catalyst (MMg$\rightarrow$MMgO reaction (9) using N_2O instead of CO_2), alternative oxidizing agents are highly recommended to promote a catalytic cycle in which both CH_4 and CO_2 are consumed at ambient conditions for the production of valuable chemicals.

The problem of finding a catalyst that is capable of activating methane and CO_2 simultaneously can tellingly be exemplified with regard to oxygen-atom transfer catalysis from carbon dioxide to methane. Thus, to enable CO_2 activation in terms of OAT from CO_2 to the cluster [reactions (7)–(11)] without using an external energy source, the cluster must have a higher OAA than CO (532 kJ mol^{-1}); In contrast, a lower OAA than that of methane (379 kJ mol^{-1}) is required to achieve exothermic OAT from the cluster to methane [reactions (2) and (13)]. Accordingly, analysis of the reaction enthalpies of reactions involving CH_4 and CO_2 activations reveals that promising species with regard to CO_2 activation are relatively poor mediators, with respect to the activation of methane; this holds true for all processes except reactions (4) and (5). To mediate the coupling of CO_2 and methane at ambient conditions, a balance of the OAA of the cluster oxides is required to accomplish oxygen donating and accepting steps; this is not possible without using additional oxygenating species, such as N_2O. In this sense, seeking a "simple" reagent (a single-site catalyst)[16] to simultaneously bring about activation and coupling of CH_4 and CO_2 with high efficiency seems extremely daunting, if not impossible.

3.5 Kinetic aspects

In the following, we focus our attention on kinetic aspects of the HAT reaction of dioxides $[MMgO_2]^+$ with methane [reaction (12)], because HAT corresponds to the most simple reaction in which only one C–H bond of methane is cleaved and only one new bond is generated (O–H or M–H); we confine ourselves to the cationic species for which reaction (12) is more exothermic, as compared to the neutral and anionic cluster oxides.

The apparent barriers for HAT, as well as the HAT reaction enthalpies, as obtained at the B3LYP/Q level are shown in Figure 5. As obvious from Figure 5, the energy barriers and the reaction enthalpies decrease similarly in the case of the heteronuclear cluster oxides containing middle to late 3d transition metals. Interestingly, the apparent barriers are negative for the

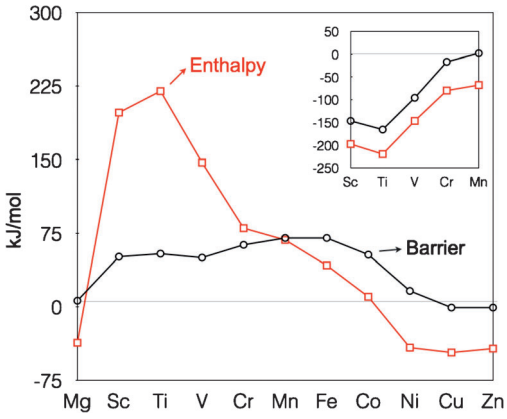

Figure 5. Reaction enthalpies and HAT apparent barriers for the reaction $[MMgO_2]^+ + CH_4 \rightarrow [MMgO_2H]^+ + CH_3^{\cdot}$ as a function of the dopant metal M. Inset shows the reverse reaction (12) for M = Sc–Mn.

Cu- and Zn-doped oxides. In contrast, the correlation between the reaction enthalpy and the barrier is not observed for cluster oxides containing early to middle 3d transition metals, because these reactions are rather endothermic. However, regarding the reverse reaction, $[MMgO_2H]^+ + CH_3 \rightarrow [MMgO_2]^+ + CH_4$, a good correlation between the energies of the barriers (relative to the separated reactants $[MMgO_2H]^+ + CH_3$) and the reaction enthalpies is, as expected, clearly observed, in line with Hammond's postulate.[17]

4. Conclusion

This computational survey provides a coherent reactivity picture using thermodynamic and kinetic descriptors to shed light on a series of CH_4 and CO_2 reactions mediated by $[MMgO]^{+/0/-}$ (M = Sc-Zn). Quite a few interesting trends have been identified: for methane activation, the late 3d transition metal doped metal oxide clusters are more promising; in contrast, for CO_2 activation, cluster oxides containing early 3d transition metals are more suitable. A linear correlation between thermodynamic and kinetic data has been established for the $[MMgO_2]^+$ mediated HAT from methane. Likewise, the doping effects[18] of the 3d transition metals, the roles of charge and oxidation states towards both CH_4 and CO_2 activation have been elucidated. Although our conclusions are drawn from the reactions of 3d transition-metal doped magnesium oxides, they may represent general reactivity patterns.

It is obvious from this study that the trends in the thermochemistry are very different for the activation of CO_2 and CH_4—actually, they oppose each other. Thus, the prospects to accomplish CH_4 and CO_2 coupling with a single-site catalyst are far from promising. Rather, an alternative method, aimed at designing a multifunctional catalyst, is indicated, in which one part promotes the C–H bond activation of methane and the other is involved in the activation of CO_2. Of course, ideally these two "hands" should work in concert.[2b] For example, a CH_4-reactive site should contain a late 3d transition-metal center, whereas the CO_2-activating site should employ an early 3d transition metal; this may help to accomplish the coupling

reaction irrespective of the overall reaction thermochemistry. In fact, this co-operative action of two metal sites has been demonstrated in the coupling of CH_4 and NH_3 to form HCN by employing the heteronuclear clusters $[MPt]^+$ (M = Cu, Ag, or Au). Here, platinum is crucial for the activation of CH_4, while the role of the coinage metal M is confined to affecting the branching ratio of the C–N bond coupling step versus unwanted soot formation.[19]

5. Computational details

All calculations were performed with the Gaussian 09 package.[20] To obtain global minima for each species under investigation, various possible starting structures were considered. For molecules having more than one possible isomer, the structure with the lowest electronic energy was singled out and used in the ensuing calculations. The geometries of all structures were optimized by employing the B3LYP hybrid density functional,[21] which is not only the most widely used density functional, but also has a well-documented accuracy performance: For molecules containing first- and second-row atoms, the error bars rarely exceed $\pm 13\ kJ\,mol^{-1}$; for transition metal-containing systems, the accuracy is normally confined to $\pm 21\ kJ\,mol^{-1}$.[22] All geometries were fully optimized without symmetry constraints, and for all elements, the def2-QZVP(Q) basis set was employed in the optimization.[23] Harmonic vibrational frequencies were computed to verify the nature of the stationary points; all minimum structures reported here possess positive eigenvalues of the Hessian matrix. Furthermore, various spin multiplicities were considered for each species. It should be noted that for systems having energetically comparable low-lying spin states, the different basis sets may assign different spin states as ground state. As the energies of these near-degenerate states are often rather close, the energetics between these different spin states do not affect dramatically the calculations of the thermodynamic properties.[24] Although a recent study indicates that there is no single DFT functional that gives good results for a wide-range of systems,[25] benchmark studies show that B3LYP has a robust, high performance for 3d transition metals as well as for M–H,[26] M–C[27] and M–O interactions.[24,28] Thus, as the focus of this study is on identifying qualitative trends rather than on a quantitative description, this computational approach is deemed acceptable.

Unscaled vibrational frequencies were used to calculate zero-point energy (ZPE) contributions, and thermal correction terms to the enthalpy ($\Delta_r H$) were estimated within the ideal gas, rigid-rotor, and harmonic oscillator approximation at a temperature of 298 K and a pressure of 1 atm. Population analysis (charge and spin density) has been performed by applying Bader's quantum theory of atoms in molecules (QTAIM).[29] The program Multiwfn was employed for these purposes.[30]

The geometries, multiplicities of lowest-energy structures and atomic charges, and available experimental data are contained in the Supporting Information.

Acknowledgements

This research was sponsored by the Deutsche Forschungsgemeinschaft (DFG), in particular the Cluster of Excellence "Unifying Concepts in Catalysis" (UniCat; coordinated by the Technische Universität Berlin and funded by the DFG), and the Fonds der Chemischen Industrie. Dr. J. Li is grateful to "UniCat" for a postdoctoral fellowship, and Dr. P. González-Navarrete acknowledges support from the Alexander von Humboldt Foundation in the form of a Postdoctoral Research Fellowship.

Keywords: carbon dioxide · computational chemistry · kinetics · methane · thermodynamics

[1] F. Fischer, H. Tropsch, *Brennst.-Chem.* **1928**, *3*, 39–46.

[2] a) L. Shi, G. H. Yang, K. Tao, Y. Yoneyama, Y. S. Tan, N. Tsubaki, *Acc. Chem. Res.* **2013**, *46*, 1838–1847; b) J.-F. Wu, S.-M. Yu, W. D. Wang, Y.-X. Fan, S. Bai, C.-W. Zhang, Q. Gao, J. Huang, W. Wang, *J. Am. Chem. Soc.* **2013**, *135*, 13567–13573; c) Y. H. Hu in *ACS Symposium Series, Vol. 1056: Advances in CO_2 Conversion and Utilization* (Ed.: Y. H. Hu), American Chemical Society, Washington, DC, **2010**, Chapter 10.

[3] J. A. Manion, R. E. Huie, R. D. Levin, D. R. B., Jr., V. L. Orkin, W. Tsang, W. S. McGivern, J. W. Hudgens, V. D. Knyazev, D. B. Atkinson, E. Chai, A. M. Tereza, C.-Y. Lin, T. C. Allison, W. G. Mallard, F. Westley, J. T. Herron, R. F. Hampson, D. H. Frizzell, NIST Chemical Kinetics Database, NIST Standard Reference Database 17, Version 17.10 (Web Version), Release 11.16.18, Data version 2013.03, National Institute of Standards and Technology, Gaithersburg, Maryland, 20899–28320. Web address: http://kinetics.nist.gov/.

[4] a) X.-N. Wu, X.-N. Li, X.-L. Ding, S.-G. He, *Angew. Chem. Int. Ed.* **2013**, *52*, 9952–9955; *Angew. Chem.* **2013**, *125*, 10136–10139; b) L. Xu, H. Song, L. Chou, *ACS Catal.* **2012**, *2*, 1331–1342.

[5] a) K. Teramura, T. Tanaka, H. Ishikawa, Y. Kohno, T. Funabiki, *J. Phys. Chem. B* **2003**, *107*, 346–354; b) R. J. Rollason, J. M. C. Plane, *Phys. Chem. Chem. Phys.* **2001**, *3*, 4733–4740.

[6] a) P. Schwach, M. G. Willinger, A. Trunschke, R. Schlögl, *Angew. Chem. Int. Ed.* **2013**, *52*, 11381–11384; *Angew. Chem.* **2013**, *125*, 11591–11594; b) K. Kwapien, M. Sierka, J. Döbler, J. Sauer, *ChemCatChem* **2010**, *2*, 819–826; c) V. García, J. J. Fernández, W. Ruíz, F. Mondragón, A. Moreno, *Catal. Commun.* **2009**, *11*, 240–246; d) R. Bouarab, O. Akdim, A. Auroux, O. Cherifi, C. Mirodatos, *Appl. Catal. A* **2004**, *264*, 161–168; e) C.-W. Hu, H.-Q. Yang, N.-B. Wong, Y.-Q. Chen, M.-C. Gong, A.-M. Tian, C. Li, W.-K. Li, *J. Phys. Chem. A* **2003**, *107*, 2316–2323; f) R. H. Nibbelke, J. Scheerova, M. H. J. M. Decroon, G. B. Marin, *J. Catal.* **1995**, *156*, 106–119.

[7] a) W. J. Jang, D. W. Jeong, J. O. Shim, H. S. Roh, I. H. Son, S. J. Lee, *Int. J. Hydrogen Energy* **2013**, *38*, 4508–4512; b) J. G. Zhang, H. Wang, A. K. Dalai, *Ind. Eng. Chem. Res.* **2009**, *48*, 677–684; c) H. Y. Wang, E. Ruckenstein, *Appl. Catal. A* **2001**, *209*, 207–215; d) K.-i. Aika, T. Nishiyama, *J. Chem. Soc. Chem. Commun.* **1988**, 70–71.

[8] a) P. Myrach, N. Nilius, S. V. Levchenko, A. Gonchar, T. Risse, K.-P. Dinse, L. A. Boatner, W. Frandsen, R. Horn, H.-J. Freund, R. Schlögl, M. Scheffler, *ChemCatChem* **2010**, *2*, 854–862; b) C. H. Lin, T. Ito, J. Wang, J. H. Lunsford, *J. Am. Chem. Soc.* **1987**, *109*, 4808–4810.

[9] K. Kwapien, J. Paier, J. Sauer, M. Geske, U. Zavyalova, R. Horn, P. Schwach, A. Trunschke, R. Schlögl, *Angew. Chem. Int. Ed.* **2014**, *53*, 8774–8778.

[10] X. Zhang, H. Schwarz, *ChemCatChem* **2010**, *2*, 1391–1394.

[11] K.-C. Lau, B. J. Petro, S. Bontemps, R. F. Jordan, *Organometallics* **2013**, *32*, 6895–6898.

[12] a) X.-N. Wu, S.-Y. Tang, H.-T. Zhao, T. Weiske, M. Schlangen, H. Schwarz, *Chem. Eur. J.* **2014**, *20*, 6672–6677; b) H. Schwarz, *Isr. J. Chem.* **2014**, *54*, 1413–1431; c) Z.-C. Wang, J.-W. Liu, M. Schlangen, T. Weiske, D. Schröder, J. Sauer, H. Schwarz, *Chem. Eur. J.* **2013**, *19*, 11496–11501; d) J.-B. Ma, Z.-C. Wang, M. Schlangen, S.-G. He, H. Schwarz, *Angew. Chem. Int. Ed.* **2013**, *52*, 1226–1230; *Angew. Chem.* **2013**, *125*, 1264–1268; e) N. Dietl, T. Wende, K. Chen, L. Jiang, M. Schlangen, X. Zhang, K. R. Asmis, H. Schwarz, *J. Am. Chem. Soc.* **2013**, *135*, 3711–3721; f) N. Dietl, X. H. Zhang, C. van der Linde, M. K. Beyer, M. Schlangen, H. Schwarz, *Chem. Eur. J.* **2013**, *19*, 3017–3028; g) J.-B. Ma, Z.-C. Wang, M. Schlangen, S.-G. He, H. Schwarz, *Angew. Chem. Int. Ed.* **2012**, *51*, 5991–5994; *Angew. Chem.* **2012**, *124*, 6093–6096; h) Z. C. Wang, N. Dietl, R. Kretschmer, J. B. Ma, T. Weiske, M. Schlangen, H. Schwarz, *Angew. Chem. Int. Ed.* **2012**, *51*, 3703–3707; *Angew. Chem.* **2012**, *124*, 3763–3767; i) N. Dietl, M. Schlangen, H. Schwarz, *Angew. Chem. Int. Ed.* **2012**, *51*, 5544–5555; *Angew. Chem.* **2012**, *124*, 5638–5650; j) N. Dietl, R. F. Höckendorf, M. Schlangen,

M. Lerch, M. K. Beyer, H. Schwarz, *Angew. Chem. Int. Ed.* **2011**, *50*, 1430 – 1434; *Angew. Chem.* **2011**, *123*, 1466 – 1470; k) N. Dietl, R. Paul, C. Linde, M. Schlangen, M. K. Beyer, H. Schwarz, *Angew. Chem. Int. Ed.* **2011**, *50*, 4966 – 4969; *Angew. Chem.* **2011**, *123*, 5068 – 5072; l) Z.-C. Wang, N. P. R. Dietl, R. Kretschmer, T. Weiske, M. Schlangen, H. Schwarz, *Angew. Chem. Int. Ed.* **2011**, *50*, 12351 – 12354; *Angew. Chem.* **2011**, *123*, 12559 – 12562; m) Y.-X. Zhao, X.-N. Wu, J.-B. Ma, S.-G. He, X.-L. Ding, *Phys. Chem. Chem. Phys.* **2011**, *13*, 1925 – 1938; n) Z.-C. Wang, T. Weiske, R. Kretschmer, M. Schlangen, M. Kaupp, H. Schwarz, *J. Am. Chem. Soc.* **2011**, *133*, 16930 – 16937; o) H. Schwarz, *Angew. Chem. Int. Ed.* **2011**, *50*, 10096 – 10115; *Angew. Chem.* **2011**, *123*, 10276 – 10297; p) X.-L. Ding, X.-N. Wu, Y.-X. Zhao, S.-G. He, *Acc. Chem. Res.* **2011**, *44*, 382 – 390; q) K. Chen, Z.-C. Wang, M. Schlangen, Y.-D. Wu, X. Zhang, H. Schwarz, *Chem. Eur. J.* **2011**, *17*, 9619 – 9625; r) J.-B. Ma, X.-N. Wu, X.-X. Zhao, X.-L. Ding, S.-G. He, *Phys. Chem. Chem. Phys.* **2010**, *12*, 12223 – 12228; s) N. P. R. Dietl, M. Engeser, H. Schwarz, *Chem. Eur. J.* **2010**, *16*, 4452 – 4456; t) N. P. R. Dietl, M. Engeser, H. Schwarz, *Angew. Chem. Int. Ed.* **2009**, *48*, 4861 – 4863; *Angew. Chem.* **2009**, *121*, 4955 – 4957; u) S. Feyel, J. Döbler, R. F. Höckendorf, M. K. Beyer, J. Sauer, H. Schwarz, *Angew. Chem. Int. Ed.* **2008**, *47*, 1946 – 1950; *Angew. Chem.* **2008**, *120*, 1972 – 1976; v) S. Feyel, D. Schröder, X. Rozanska, J. Sauer, H. Schwarz, *Angew. Chem. Int. Ed.* **2006**, *45*, 4677 – 4681; *Angew. Chem.* **2006**, *118*, 4793 – 4797; w) S. Feyel, J. Döbler, D. Schröder, J. Sauer, H. Schwarz, *Angew. Chem. Int. Ed.* **2006**, *45*, 4681 – 4685; *Angew. Chem.* **2006**, *118*, 4797 – 4801.

[13] a) X.-N. Wu, Y.-X. Zhao, W. Xue, Z.-C. Wang, S.-G. He, X.-L. Ding, *Phys. Chem. Chem. Phys.* **2010**, *12*, 3984 – 3997; b) I. Kretzschmar, A. Fiedler, J. N. Harvey, D. Schröder, H. Schwarz, *J. Phys. Chem. A* **1997**, *101*, 6252 – 6264.

[14] Z.-Y. Li, Y.-X. Zhao, X.-N. Wu, X.-L. Ding, S.-G. He, *Chem. Eur. J.* **2011**, *17*, 11728 – 11733.

[15] a) A. Rit, T. P. Spaniol, J. Okuda, *Chem. Asian J.* **2014**, *9*, 612 – 619; b) H. Tang, C. Wu, *ChemSusChem* **2013**, *6*, 1050 – 1056; c) W. Sattler, G. Parkin, *J. Am. Chem. Soc.* **2012**, *134*, 17462 – 17465; d) D. J. Darensbourg, A. Rokicki, M. Y. Darensbourg, *J. Am. Chem. Soc.* **1981**, *103*, 3223 – 3224.

[16] a) K. Horn, *Science* **2004**, *305*, 483 – 484; b) J. M. Thomas, *Angew. Chem. Int. Ed.* **2005**, *44*, 5563 – 5566; *Angew. Chem.* **2005**, *117*, 5699 – 5702; c) R. Horn, R. Schlögl, *Catal. Lett.* **2015**, *145*, 23 – 39.

[17] G. S. Hammond, *J. Am. Chem. Soc.* **1955**, *77*, 334 – 338.

[18] For a recent review on doping effects in the gas-phase chemistry and physics of heteronuclear metal oxides, see: H. Schwarz, *Angew. Chem. Int. Ed.* **2015**, DOI: 10.1002/anie.201500649; *Angew. Chem.* **2015**, DOI: 10.1002/ange.201500649.

[19] K. Koszinowski, D. Schröder, H. Schwarz, *Angew. Chem. Int. Ed.* **2004**, *43*, 121 – 124; *Angew. Chem.* **2004**, *116*, 124 – 127.

[20] M. J. Frisch, G. W. Trucks, H. B. Schlegel, G. E. Scuseria, M. A. Robb, J. R. Cheeseman, G. Scalmani, V. Barone, B. Mennucci, G. A. Petersson, H. Nakatsuji, M. Caricato, X. Li, H. P. Hratchian, A. F. Izmaylov, J. Bloino, G. Zheng, J. L. Sonnenberg, M. Hada, M. Ehara, K. Toyota, R. Fukuda, J. Hasegawa, M. Ishida, T. Nakajima, Y. Honda, O. Kitao, H. Nakai, T. Vreven, J. J. A. Montgomery, J. E. Peralta, F. Ogliaro, M. Bearpark, J. J. Heyd, E. Brothers, K. N. Kudin, V. N. Staroverov, T. Keith, R. Kobayashi, J. Normand, K. Raghavachari, A. Rendell, J. C. Burant, S. S. Iyengar, J. Tomasi, M. Cossi, N. Rega, J. M. Millam, M. Klene, J. E. Knox, J. B. Cross, V. Bakken, C. Adamo, J. Jaramillo, R. Gomperts, R. E. Stratmann, O. Yazyev, A. J. Austin, R. Cammi, C. Pomelli, J. W. Ochterski, R. L. Martin, K. Morokuma, V. G. Zakrzewski, G. A. Voth, P. Salvador, J. J. Dannenberg, S. Dapprich, A. D. Daniels, O. Farkas, J. B. Foresman, J. V. Ortiz, J. Cioslowski, D. J. Fox, Gaussian 09, Revision D.01, Gaussian, Inc., Wallingford CT, **2013**.

[21] a) A. D. Becke, *J. Chem. Phys.* **1993**, *98*, 5648 – 5652; b) C. Lee, W. Yang, R. G. Parr, *Phys. Rev. B* **1988**, *37*, 785 – 789.

[22] P. E. M. Siegbahn, T. Borowski, *Acc. Chem. Res.* **2006**, *39*, 729 – 738.

[23] F. Weigend, R. Ahlrichs, *Phys. Chem. Chem. Phys.* **2005**, *7*, 3297 – 3305.

[24] X. Zhang, H. Schwarz, *Theor. Chem. Acc.* **2011**, *129*, 389 – 399.

[25] J. L. Li, R. A. Mata, U. Ryde, *J. Chem. Theory Comput.* **2013**, *9*, 1799 – 1807.

[26] a) V. Barone, C. Adamo, *Int. J. Quantum Chem.* **1997**, *61*, 443 – 451; b) D. Rinaldo, L. Tian, J. N. Harvey, R. A. Friesner, *J. Chem. Phys.* **2008**, *129*, 164108.

[27] X. Zhang, H. Schwarz, *Chem. Eur. J.* **2010**, *16*, 5882 – 5888.

[28] J. Li, S. Tang, M. Schlangen, H. Schwarz, unpublished results.

[29] R. F. W. Bader, *Atoms in Molecules: A Quantum Theory*, Oxford University Press, New York, **1994**.

[30] T. Lu, F. Chen, *J. Comput. Chem.* **2012**, *33*, 580 – 592.

Received: February 19, 2015
Published online on ■■ ■■, 0000

FULL PAPER

Mission: Impossible? DFT calculations show that the trends in the thermochemistry are very different for the activation of CO_2 and CH_4 mediated by transition-metal doped magnesium oxide clusters $[MMgO]^{+/0/-}$ (M = Sc–Zn). Thus, seeking a "simple" reagent to simultaneously mediate activation and coupling of CH_4 and CO_2 with high efficiency seems extremely daunting, if not impossible.

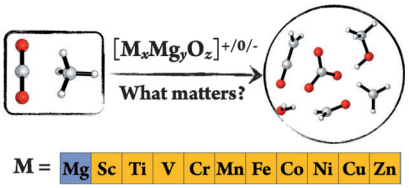

Density Functional Calculations

*J. Li, P. González-Navarrete, M. Schlangen, H. Schwarz**

■■ – ■■

Activation of Methane and Carbon Dioxide Mediated by Transition-Metal Doped Magnesium Oxide Clusters $[MMgO]^{+/0/-}$ (M = Sc–Zn)